



OPEN

A compact wideband antenna with high gain based on spoof surface plasmon polaritons

Farshad Arghandeh, Bijan Abbasi-Arand & Maryam Hesari-Shermeh

In this paper, a novel wideband antenna with a simple structure and low profile based on spoof surface plasmon polaritons (SSPPs) is proposed. The structure consists of periodically modulated corrugated metal strips as transmission lines, a CPW feed, and a ground metal plate as an antenna reflector. The SSPP transmission line is used to convert quasi-TEM to SSPP mode and achieve optimal impedance matching. The prototype of the end-fire antenna has been designed and fabricated. The simulation results show that this antenna can achieve a gain of 10.19 dB, a bandwidth of 146%, and an efficiency of 90% in a wide operating band from 7 to 45 GHz. The proposed design illustrates great potential that includes high efficiency, good directivity, high gain, wide bandwidth, and easy manufacturing.

Keywords Wideband, End-fire, Spoof surface plasmon polaritons (SSPP)

Surface plasmon polaritons (SPP) are light waves that can be propagated at the interface between a metal and a dielectric^{1–3}. Since the metals in microwave frequencies behave as perfect electrical conductors (PEC) with negative permittivity, SPPs are not produced in these frequencies^{4,5}. However, to take advantage of the properties of SPP modes at microwave frequencies, metamaterials are presented to achieve novel surface responses that have similar properties to SPP modes. In 2004, Pendry et al.⁶ designed an array structure consisting of periodic subwavelength cubic holes on a metal surface, which is referred to as a spoof structure. A spoof surface plasmon polariton (SSPP) has been fabricated using plasmonic metamaterials with alternating sheet metal structures, which exhibit SPP's behavior at microwave and terahertz frequencies⁷.

One of the key advantages of this metamaterial is that the geometrical parameters of the elements can control the dispersion and spatial confinement characteristics of SSPPs. These advantages make SSPPs good candidates for high-density integrated circuits and components at millimeter-wave and terahertz frequencies^{8,9}. Significant advancements have been achieved in this area, including the development of transmission structures utilizing coplanar waveguide (CPW) or microstrip lines^{10–12}, advancements in filter technology^{8,13}, the design of power dividers¹⁴, and innovation in antennas^{15–23}. In¹⁶, an end-fire antenna was proposed, utilizing a structure based on SSPPs with metamaterial particles. In this design, the main radiator is a printed dipole, while the SSPP waveguide serves as a feed structure for the printed dipole. The configuration includes an I-shaped resonator array to achieve a high effective refractive index, resulting in enhanced gain in the desired end-fire direction. Moreover, in¹⁷, a near-end fire wideband antenna was introduced, utilizing SSPPs with metamaterial H-shaped cells, while in¹⁸, an end-fire antenna utilizing SSPPs was proposed. To achieve the excitation of the printed dipole, a pair of SSPP waveguides was printed on both the upper and lower layers of the substrate. In¹⁹, a wideband end-fire antenna with a fishbone shape was designed, utilizing SSPPs. The feeding structure of that antenna comprised a microstrip-to-slit converter and a differential mode exciter, enabling the excitation of the odd mode signal on the SSPPs. In²⁰, a small aperture end-fire antenna was designed using odd-mode SSPPs, and the SSPP antenna was constructed using dipole unit cells. The antenna presented in²¹ employed a printed dipole as the primary radiator while, additionally, shape resonators and parasitic bands were incorporated in the direction of the end-fire to enhance directionality. However, due to the inherent resonant characteristics of the dipole, the bandwidth of that end-fire antenna was limited, resulting in a lower gain and front-to-back ratio. Furthermore, in²², a near-end fire antenna based on SSPPs was presented, where the objective of that paper was to design a high-gain antenna within the frequency range of 7.5 to 8.5 GHz. In²³, a high-gain SSPP-based broadband antenna is proposed, in which the SSPP waveguide is composed of a very thin corrugated metal strip and a dielectric substrate layer. To improve the SSPP antenna directivity, a director is also loaded at the end of the antenna. The proposed antenna has a bandwidth of 65% and a maximum gain of 6.6 dBi.

Department of Electrical and Computer Engineering, Tarbiat Modares University, Tehran 14115-194, Iran. email: abbasi@modares.ac.ir

In this paper, a novel wideband antenna is introduced using an SSPP structure. In this design, a wide impedance bandwidth ranging from 7 to 45 GHz is achieved using a semi-circular unit cell, two metal plates as the antenna ground, a CPW feed, and an SSPP transmission line. The semi-circular slits are designed to match the characteristic impedance of the CPW to the SSPP transmission line and then reduce the reflection. Moreover, the proposed unit cell provides the conditions for creating a slow wave and reduced reflection, which leads to better impedance matching. By utilizing the SSPP transmission line, the antenna shows better field confinement and higher efficiency. The proposed antenna has been designed, simulated, and fabricated, and the results show that the novel end-fire antenna has the advantages of a wide impedance bandwidth (146%), high efficiency (90%), high gain (10.19 dB), and a compact size.

Design implications

The configuration of the proposed antenna is illustrated in Fig. 1. This antenna has been designed on a Rogers RT5880 substrate with $\epsilon_r = 2.2$ and $\tan\delta = 0.0009$, and a thickness of $t = 0.5$ mm. The optimal antenna parameters are presented in Table 1.

The proposed antenna consists of three main parts: a CPW feed, an SSPP transmission line, and a tapering area. The CPW feed plays a crucial role in the antenna's functionality as its primary function is to convert the quasi-TEM mode into the SSPP transmission line. Additionally, it serves as a wavelength transformer to achieve impedance matching between the SSPP transmission line and the 50Ω port. The SSPP transmission line has been used as a transmission line for the excitation of the end-fire antenna due to its advantages such as field confinement, low loss, controllable dispersion, and slow wave. The half-circular tapering region at the end of the antenna is used to convert the TM waves propagated in the SSPP transmission line into free-space propagation waves, and by using a tapering area at the end of the antenna, a wide impedance bandwidth is achieved.

In summary, the wideband characteristic of the proposed antenna design is realized through a combination of key design elements and careful optimization. The antenna design utilizes a CPW feed, an SSPP transmission line, and a tapering area to achieve its wideband operation. The SSPP transmission line provides field confinement, low loss, controllable dispersion, and slow wave, which contribute to the wideband operation of the antenna. The geometry of the unit cell, the length of the tapering half-circles, and the total length of the transmission line cells have been carefully optimized to minimize reflections and impedance variations while maximizing antenna performance. These optimizations are critical for achieving the wideband characteristic of the antenna. Furthermore, the tapering area at the end of the antenna is used to convert the TM waves propagated in the SSPP transmission line into free-space propagation waves, enabling a wide impedance bandwidth.

The geometry of the half-circular unit cell is defined by two parameters: the radius (R) and the total height (S) of the structure. The proposed antenna operates based on the Hanson-Woodyard²⁴ condition, which indicates that not only the terminal part but also the initial and body parts contribute to enhancing the radiation. Also, according to the Hanson-Woodyard condition, the optimal guided phase constant should be slightly larger

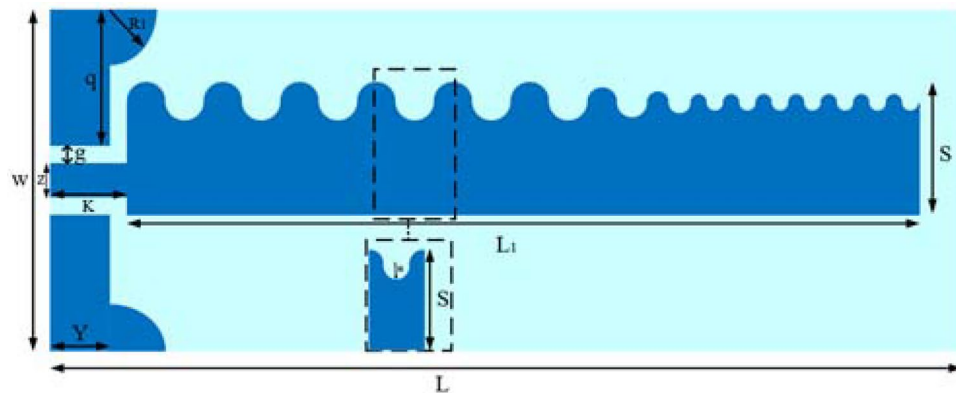


Figure 1. Schematic of our proposed antenna, based on SSPP.

Parameter	Value	Parameter	Value
W	30 mm	g	0.7 mm
L	80 mm	Z	2.6 mm
Y	4.3 mm	K	5 mm
q	13 mm	S	10 mm
R	2 mm	$L1$	72 mm
$R1$	4.5 mm		

Table 1. Optimum parameters of the SSPP-based antenna.

than that in air. Therefore, the spray curve should remain a short distance below the air line. Figure 2 shows the dispersion curve of the unit cell for varying groove depths, and as illustrated in the figure, the dispersion curve of the SSPP transmission line exhibits a deviation from the light line. This indicates the presence of a slow-wave phenomenon in this structure. As the value of R increases, the field confinement around the SSPP transmission line becomes stronger, resulting in enhanced radiation, improved impedance bandwidth, and increased antenna gain. Moreover, due to the increase in R value from a certain point onward, the spray curve moves away from the air line. Consequently, this results in diminished phase matching between the structure and free space for radiation. Likewise, the value of R significantly influences the impedance matching performance, where Fig. 3 shows the effect of the depth of the groove on the impedance matching. Therefore, there is an optimal groove depth ($R = 2$ mm) in the desired frequency range.

The height of the tapering half-circles gradually changes with a step of 0.5 mm, within the range of 1.5 mm to 0.5 mm. The value of S also plays a crucial role in impedance matching, and its optimal value is $S = 10$ mm. The SSPP transmission line, the tapered area at the end of the antenna, and the value of S were optimized to minimize reflections and impedance variations. Furthermore, the length of $L1$ has been carefully selected to achieve two goals: reducing reflections and improving impedance matching without increasing the size of the antenna. Hence, the optimal value for $L1$ is determined to be 72 mm. It is important to mention that to finalize the remaining dimensions of the proposed antenna, all the parameters have been determined based on thoroughly examination and extensive simulations. To optimize the antenna's response, it is crucial to take into account the structural size of each component and its impact on the overall performance of the antenna. Therefore, it is essential to optimize the number of transmission line cells to achieve the best results. Figure 4 illustrates the variation in maximum antenna gain with respect to the total length, represented by the number of SSPP transmission line cells. The gain shows an increase from 5.8 dB to 10.19 dB as the antenna length increases. Notably, when the length ratio

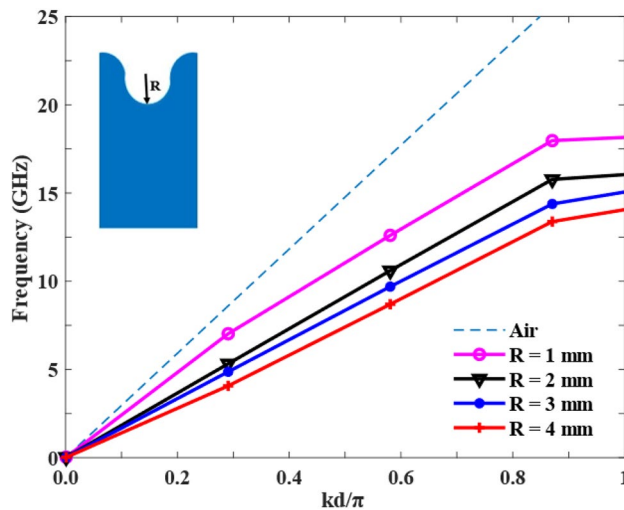


Figure 2. Dispersion curve of the unit cell.

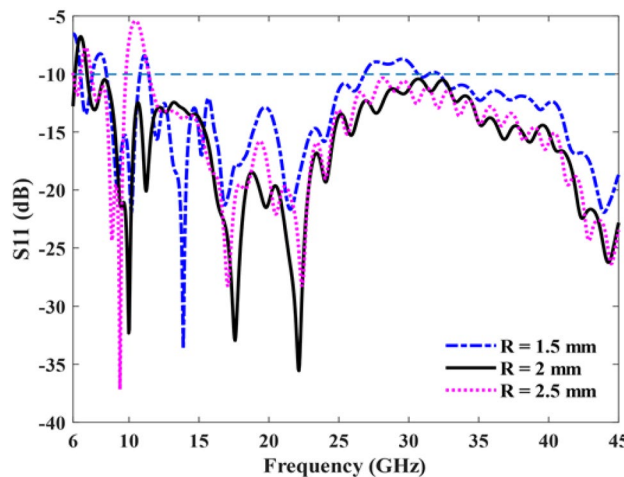


Figure 3. Antenna S11 for different values of R .

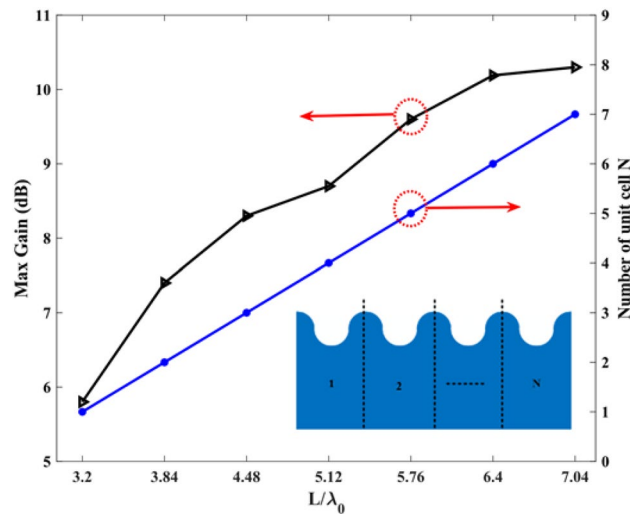


Figure 4. Total length versus maximum gain and number of unit cells (N), where λ_0 is the wavelength at 24 GHz.

L/λ_0 exceeds 6.4, there is a slight increase in the maximum gain. Based on this observation, a transmission line consisting of six unit cells was selected to achieve the highest gain while maintaining a minimal antenna size. Consequently, the total length of the line has been determined as $L = 80$ mm. Also, Fig. 5 shows the reflection coefficients of the antenna per unit cell number. As can be seen, the reflection coefficients of the antenna per 6 cells have better impedance matching than others.

Figure 6 illustrates the reflection coefficients of the antenna with and without the half-circle introduced in front of the antenna's ground plane. The half-circle acts as a reflector, causing transmitted energy to reflect back and this results in improved reflection coefficients, particularly at lower frequencies. The reflection coefficients of the antenna without the half-circle are observed within the frequency range of 11.1 to 45 GHz, whereas the antenna with the half-circle exhibits better impedance matching in the frequency range of 7 to 45 GHz.

The proposed design has been implemented and simulated using CST software, utilizing a Rogers RT5880 substrate. Figure 7 displays the reflection coefficients of the proposed antenna, revealing that the reflection coefficients remain below -10 dB in the frequency range of 7 to 45 GHz, indicating good impedance matching within this range.

Figure 8 illustrates the gain and efficiency of the simulated antenna across the frequency range of 7 to 45 GHz where the total gain exhibits variations from 6.13 to 10.19 dB. The simulation results clearly demonstrate that the proposed antenna achieves high efficiency, averaging 90% across a wide operating band from 7 to 45 GHz. In Fig. 8, we evaluated the gain of the structure. However, upon factoring in the negative impact of reflection loss, we discovered that realized gain was 0.25 dB lower than the calculated gain.

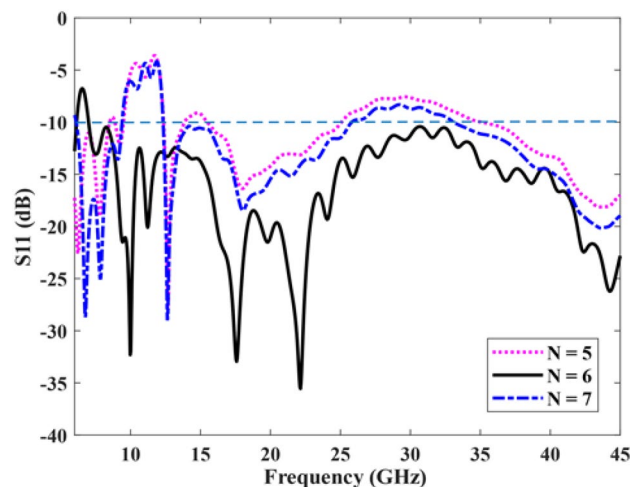


Figure 5. S11 per number of cells.

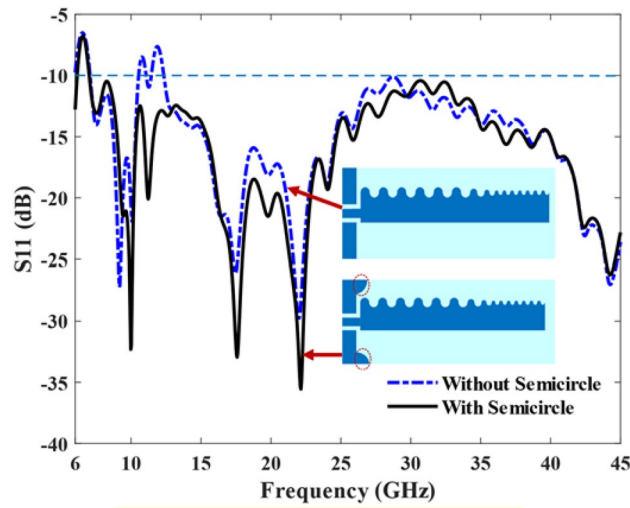


Figure 6. Antenna S11 with and without a half-circle.

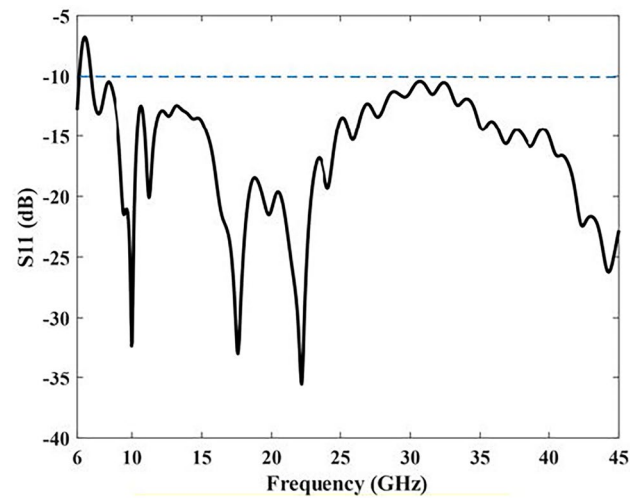


Figure 7. Simulated S11 of the proposed antenna.

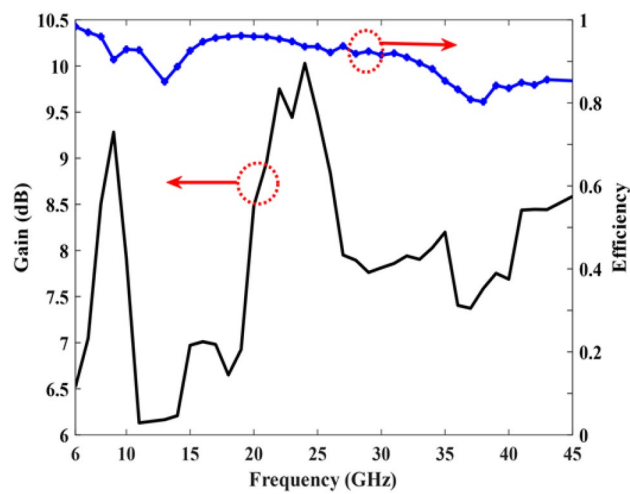


Figure 8. Simulated gain and efficiency of the proposed antenna..

Fabrication and measurement

We have designed and simulated the proposed scheme using Rogers Ro5880 substrate and have achieved an acceptable bandwidth. However, in the manufacturing phase, due to the limitation in the supply of Rogers Ro5880 substrate as well as the limitation in measurement equipment, we had to do a redesign on the Rogers Ro4003c substrate with $\epsilon_r = 3.55$, $\tan \delta = 0.0027$, and thickness of 0.5 mm, as shown in Fig. 9. Measurements on this substrate have been possible up to the maximum frequency of 22 GHz.

To accommodate the limited frequency range of the spectrum analyzer, the reflection coefficients of the proposed antenna were plotted within the frequency range of 8–22 GHz. Figure 10 shows the reflection coefficient results obtained from the simulation and measurement, which exhibited consistency with each other and confirmed the accuracy of the antenna design. The frequency deviation observed can be attributed to manufacturing errors. Notably, the reflection coefficients remained below -10 dB within the range of 8.7 to 22 GHz, indicating good impedance matching.

Figure 11 illustrates the simulated and measured antenna gain within the frequency range of 9 to 19 GHz. The total gain varies from 4.7 to 9.1 dB, and the results obtained from both simulation and measurements align with each other. Moreover, the simulated and measured normalized electric field (E) and magnetic field (H) radiation patterns at frequencies of 6 and 6.8 GHz are illustrated in Fig. 12. Table 2 depicts the comparison of our proposed antenna with other works in the literature.

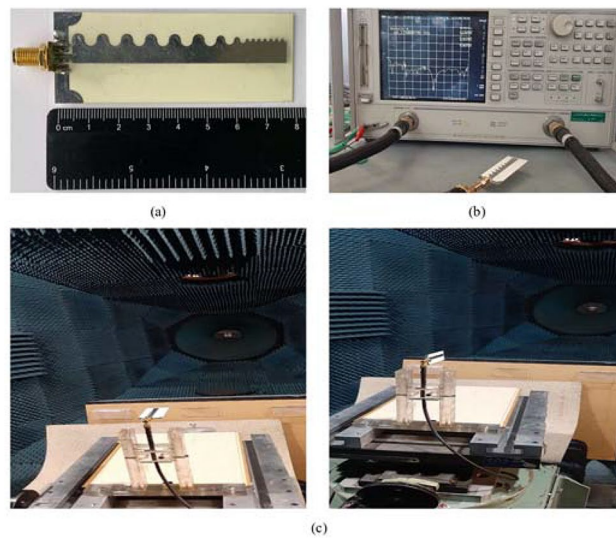


Figure 9. Prototype of the built antenna. (a) General view of the built antenna. (b) View of the antenna connected to the network analyzer. (c) View of the antenna in the antenna room.

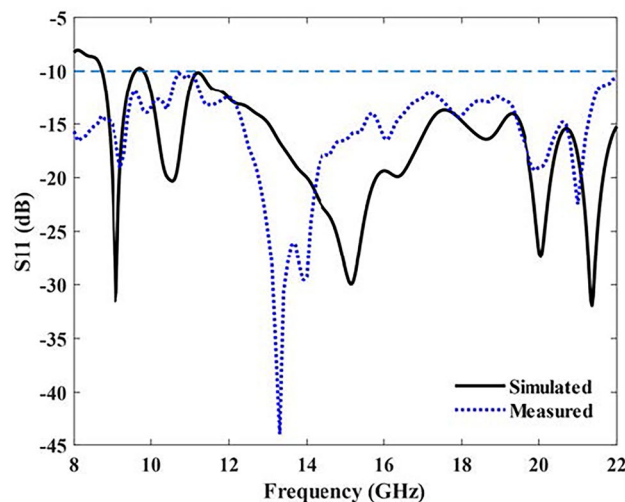


Figure 10. Simulated and measured S11 of the SSPP-based antenna.

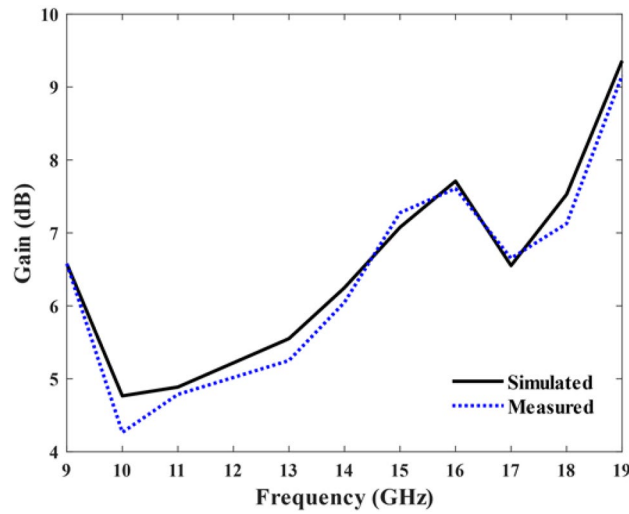


Figure 11. Simulated and measured gain of the SSPP-based antenna.

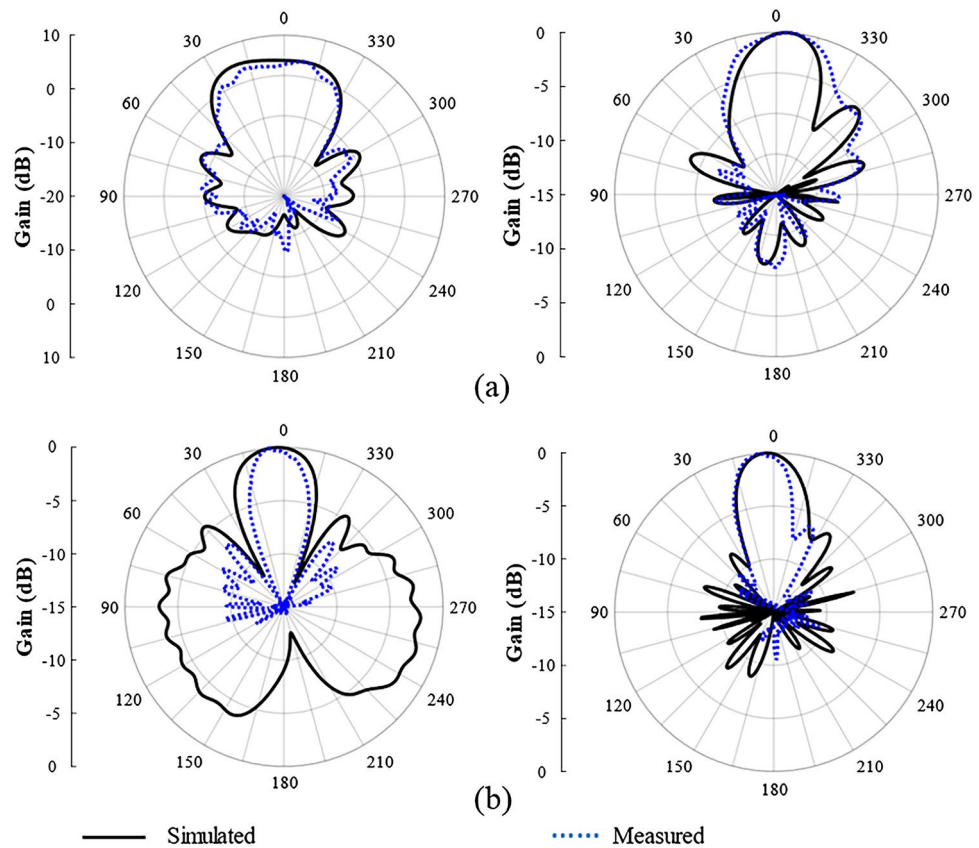


Figure 12. Simulation and measurement of the radiation fields of plane E and plane H. [(right) page E; (left) page H]. (a) 6 GHz. (b) 6.8 GHz.

Conclusion

This paper has presented the design, simulation, and fabrication of a compact antenna based on an SSPP structure, where an SSPP waveguide has been utilized for the transmission line, enabling a wide bandwidth through field confinement, slow waves, and low losses. The proposed antenna was designed on a Rogers Ro5880 substrate, yielding simulation results of a 146% bandwidth, 10.19 dB maximum gain, and 90% efficiency. However, due to manufacturing limitations and the high cost associated with the Rogers Ro5880 substrate, our proposed antenna was instead fabricated and measured on a Rogers Ro4003c substrate. The results obtained from simulation and

Ref	Bandwidth (%)	Efficiency (%)	Gain (dB)	Frequency GHz	Size (mm)
¹⁶	8.5	9.32	7	6	113 × 32
¹⁸	31	95	9.16	7	133 × 32
¹⁹	70.3	90	8.6	3.7	110 × 70
²⁰	67	54	7.9	6	116 × 40
²²	66	96	9.2	9	107 × 30
²⁵	73	87.5	12.4	9.5	75.5 × 20
²⁶	11	95	12.1	16.6	167 × 80
This Work	146	90	10.19	26	80 × 30

Table 2. A comparative analysis with other sources.

measurement on the Rogers Ro4003c substrate have demonstrated an 87% bandwidth within the frequency range of 8.5 to 22 GHz, with a maximum gain of 9.1 dB. The results obtained from simulation and measurement have also shown good agreement. Moreover, due to the unique characteristics of the SSPP transmission line, the proposed antenna demonstrates a wide bandwidth, high gain, high efficiency, and a compact size. These features position the antenna as a good candidate for wireless applications.

Data availability

The datasets generated and analyzed during the current study are available from the corresponding author on reasonable request.

Received: 12 October 2023; Accepted: 15 February 2024

Published online: 02 May 2024

References

- Ye, L. *et al.* Strongly confined spoof surface plasmon polaritons waveguiding enabled by planar staggered plasmonic waveguides. *Sci. Rep.* **6**(1), 1–8 (2016).
- Kandwal, A. *et al.* Broadband frequency scanning spoof surface plasmon polariton design with highly confined endfire radiations. *Sci. Rep.* **10**(1), 1–10 (2020).
- Ping, R., Ma, H. & Cai, Y. Compact and highly-confined spoof surface plasmon polaritons with fence-shaped grooves. *Sci. Rep.* **9**(1), 12045 (2019).
- Gao, X., Che, W. & Feng, W. Novel non-periodic spoof surface plasmon polaritons with H-shaped cells and its application to high selectivity wideband bandpass filter. *Sci. Rep.* **8**(1), 2456 (2018).
- Pan, B. C., Zhao, J., Liao, Z., Zhang, H. C. & Cui, T. J. Multi-layer topological transmissions of spoof surface plasmon polaritons. *Sci. Rep.* **6**(1), 22702 (2016).
- Pendry, J., Martin-Moreno, L. & Garcia-Vidal, F. Mimicking surface plasmons with structured surfaces. *Science* **305**(5685), 847–848 (2004).
- Fu, Q., Ni, H., Luo, G. Q., Zhu, L. & Liu, L. A high aperture efficiency endfire antenna based on spoof surface plasmon polaritons. *IEEE Trans. Antennas Propag.* **71**(1), 50–57 (2022).
- Zhao, L. *et al.* A novel broadband band-pass filter based on spoof surface plasmon polaritons. *Sci. Rep.* **6**(1), 36069 (2016).
- Wang, J., Zhao, L., Hao, Z.-C., Zhang, S. & Shen, X. Integrated hybrid antenna based on spoof surface plasmon polaritons. *IEEE Access* **9**, 10797–10804 (2021).
- Liao, Z., Zhao, J., Pan, B. C., Shen, X. P. & Cui, T. J. Broadband transition between microstrip line and conformal surface plasmon waveguide. *J. Phys. D Appl. Phys.* **47**(31), 315103 (2014).
- Kianinejad, A., Chen, Z. N. & Qiu, C.-W. Low-loss spoof surface plasmon slow-wave transmission lines with compact transition and high isolation. *IEEE Trans. Microw. Theory Tech.* **64**(10), 3078–3086 (2016).
- Liang, Y., Yu, H., Zhang, H. C., Yang, C. & Cui, T. J. On-chip sub-terahertz surface plasmon polariton transmission lines in CMOS. *Sci. Rep.* **5**(1), 14853 (2015).
- Zhang, Q., Zhang, H. C., Yin, J. Y., Pan, B. C. & Cui, T. J. A series of compact rejection filters based on the interaction between spoof SPPs and CSRRs. *Sci. Rep.* **6**(1), 28256 (2016).
- Jin Zhou, Y., Yang, X.-X. & Jun Cui, T. A multidirectional frequency splitter with band-stop plasmonic filters. *J. Appl. Phys.* **115**(12), 123105 (2014).
- Tang, X.-L., Zhang, Q., Hu, S., Chen, Y. Spoof surface plasmon polaritons (SSPP) for endfire radiation, in *2018 IEEE Asia-Pacific Conference on Antennas and Propagation (APCAP)*, 2018: IEEE, pp. 414–415.
- Yin, J. Y. *et al.* Endfire radiations of spoof surface plasmon polaritons. *IEEE Antennas Wirel. Propag. Lett.* **16**, 597–600 (2016).
- Li, X., Tao, J., Li, Y., Chen, Y., Deng, C. H-shaped metamaterial loaded wideband spoof surface plasmon polaritons antenna, in *2019 Cross Strait Quad-Regional Radio Science and Wireless Technology Conference (CSQRWC)*, 2019: IEEE, pp. 1–3.
- Yang, L. *et al.* A wideband high-gain endfire antenna based on spoof surface plasmon polaritons. *IEEE Antennas Wirel. Propag. Lett.* **19**(12), 2522–2525 (2020).
- Du, X., Li, H. & Yin, Y. Wideband fish-bone antenna utilizing odd-mode spoof surface plasmon polaritons for endfire radiation. *IEEE Trans. Antennas Propag.* **67**(7), 4848–4853 (2019).
- Jiang, Y., Liu, L., Hu, Y. & Jiang, D. Wideband small aperture endfire antenna based on spoof surface plasmon polaritons. *IEEE Trans. Antennas Propag.* **69**(8), 5026–5031 (2021).
- Tian, D. *et al.* Low-profile high-efficiency bidirectional endfire antenna based on spoof surface plasmon polaritons. *IEEE Antennas Wirel. Propag. Lett.* **17**(5), 837–840 (2018).
- Kandwal, A., Zhang, Q., Tang, X.-L., Liu, L. W. & Zhang, G. Low-profile spoof surface plasmon polaritons traveling-wave antenna for near-endfire radiation. *IEEE Antennas Wirel. Propag. Lett.* **17**(2), 184–187 (2017).
- Arghandeh, F., Abbasi-Arand, B. & Hesari-Shermeh, M. A wideband and compact Quasi-Yagi antenna based on spoof surface plasmon polaritons. *Sci. Rep.* **13**(1), 11054 (2023).
- Hansen, W. W. & Woodyard, J. A new principle in directional antenna design. *Proc. Inst. Radio Eng.* **26**(3), 333–345 (1938).

- 25 Xiao, B., Tu, X., Fyffe, A., Wang, X. & Shi, Z. A compact, high gain, spoof surface plasmon polariton sawtooth end-fire antenna. *J. Mod. Opt.* **67**(7), 654–660 (2020).
- 26 Liu, L., Chen, M. & Yin, X. Single-layer high gain endfire antenna based on spoof surface plasmon polaritons. *IEEE Access.* **8**, 64139–64144 (2020).

Author contributions

F. A. conceived the idea, carried out the numerical simulations and wrote the first draft of manuscript text. B. A. A. M. H. S. discussed the proposed method and simulation results, as well as improved the manuscript presentation. All authors reviewed and approved the manuscript.

Competing interests

The authors declare no competing interests.

Additional information

Correspondence and requests for materials should be addressed to B.A.-A.

Reprints and permissions information is available at www.nature.com/reprints.

Publisher's note Springer Nature remains neutral with regard to jurisdictional claims in published maps and institutional affiliations.



Open Access This article is licensed under a Creative Commons Attribution 4.0 International License, which permits use, sharing, adaptation, distribution and reproduction in any medium or format, as long as you give appropriate credit to the original author(s) and the source, provide a link to the Creative Commons licence, and indicate if changes were made. The images or other third party material in this article are included in the article's Creative Commons licence, unless indicated otherwise in a credit line to the material. If material is not included in the article's Creative Commons licence and your intended use is not permitted by statutory regulation or exceeds the permitted use, you will need to obtain permission directly from the copyright holder. To view a copy of this licence, visit <http://creativecommons.org/licenses/by/4.0/>.

© The Author(s) 2024